J|A|C|S ARTICLES

Published on Web 05/21/2010

Donor−Acceptor Conjugates of Lanthanum Endohedral Metallofullerene and π-Extended Tetrathiafulvalene

Yuta Takano,[†,‡] M. Ángeles Herranz,[†] Nazario Martín,[*,†,⊥] Shankara Gayathri Radhakrishnan,[§] Dirk M. Guldi,[*,§] Takahiro Tsuchiya,[‡] Shigeru Nagase,[||] and Takeshi Akasaka[*,‡]

Departamento de Química Orgánica I, Facultad de Química, Universidad Complutense, E-28040 Madrid, Spain, IMDEA-Nanociencia, 28049 Madrid, Spain, Center for Tsukuba Advanced Research Alliance, University of Tsukuba, 305-8577 Ibaraki, Japan, Department of Chemistry and Pharmacy & Interdisciplinary Center for Molecular Materials (ICMM), Friedrich-Alexander-Universität Erlangen-Nürnberg, Egerlandstrasse 3, 91058 Erlangen, Germany, and Department of Theoretical and Computational Molecular Science, Institute for Molecular Science, Okazaki 444-8585, Aichi, Japan

Received February 3, 2010; E-mail: nazmar@quim.ucm.es; dirk.guldi@chemie.uni-erlangen.de; akasaka@tara.tsukuba.ac.jp

Abstract: Stable donor−acceptor conjugates (**2**, **3**) involving an endohedral metallofullerene, $La_2@I_h$-C_{80}, and π-extended tetrathiafulvalene (exTTF) have been synthesized by highly regioselective 1,3-dipolar cycloadditions of exTTF-containing azomethine ylides to the endofullerene, yielding exclusively [5,6] metallofulleropyrrolidines with C_1 symmetry in high yields (68−77%). The cyclic voltammograms (CVs) of the conjugates reveal the redox active character of the system due to the presence of both donor and acceptor groups, that is, exTTF and $La_2@I_h$-C_{80}, respectively. Furthermore, the electrochemically reversible character of the endofullerene confirms the presence of the [5,6] adduct. Despite the relatively close proximity between the exTTF and the endohedral metallofullerene (EMF), only a weak electronic interaction was observed in the ground state, as evidenced by absorption spectroscopy and CV measurements of **2** and **3**. On the other hand, in the excited state the fast formation of a radical ion-pair state (i.e., 6.0×10^{10} s^{-1}), that is, the reduction of the electron accepting $La_2@C_{80}$ and the oxidation of exTTF, evolves with lifetimes as long as several ns (3.0×10^8 s^{-1}) in toluene. Transient absorption spectroscopy experiments confirmed these observations.

Introduction

A myriad of endohedral metallofullerenes (EMFs) can be formed by the encapsulation of one or more metal atoms inside the hollow cages of fullerenes.[1] What renders EMFs particularly appealing is that the chemical and physical properties can be tuned by changing the nature and composition of the encapsulated species. Among the different types of EMFs that have been reported so far, $M_2@I_h$-C_{80} (M = La and Ce) have attracted special attention because the encapsulated metal atoms circulate three-dimensionally inside the I_h-C_{80} cages.[2,3] Since the encapsulated metal atoms are positively charged, it can be considered that the dynamic behavior of the metal atoms make a major contribution to the electronic and chemical properties of the EMFs. The availability in relatively high yields and the highest symmetry of $M_2@C_{80}$ also fascinate a large number of researchers in the fields of chemistry, physics, and materials science.

Meanwhile, fullerenes, in particular [60]fullerene, present outstanding physicochemical properties, accepting up to six electrons in solution at moderate reduction potentials to form stable anionic species and, simultaneously, exhibiting very low reorganization energies in charge-transfer reactions, that render them attractive candidates for energy conversion and energy storage.[4,5] The ability of carbon to exist in different allotropic forms has provided, in addition to C_{60}, new varieties of nanoscale size shapes with fascinating properties. Control over the rate of electron transfer (i.e., charge separation and charge recombination) has been achieved in these composite materials, either by systematically altering the donor−acceptor (D−A) spatial separation or by integrating additional electron acceptors.[6]

[†] Universidad Complutense de Madrid.
[‡] University of Tsukuba.
[§] Friedrich-Alexander-Universität Erlangen-Nürnberg.
[||] Institute for Molecular Science.
[⊥] IMDEA-Nanociencia.

(1) *Endofullereres: A New Family of Carbon Clusters*; Akasaka, T., Nagase, S., Eds.; Academic Publishers: Dordrecht, 2002.

(2) (a) Kobayashi, K.; Nagase, S.; Akasaka, T. *Chem. Phys. Lett.* **1996**, *261*, 502–506. (b) Suzuki, T.; Maruyama, Y.; Kato, T.; Kikuchi, K.; Nakao, Y.; Achiba, Y.; Kobayashi, K.; Nagase, S. *Angew. Chem., Int. Ed. Engl.* **1995**, *34*, 1094–1096. (c) Ding, J.; Yang, S. *Angew. Chem., Int. Ed. Engl.* **1996**, *35*, 2234–2235. (d) Akasaka, T.; Nagase, S.; Kobayashi, K.; Waelchli, M.; Yamamoto, K.; Funasaka, H.; Kako, M.; Hoshino, T.; Erata, T. *Angew. Chem., Int. Ed. Engl.* **1997**, *36*, 1643–1645. (e) Nishibori, E.; Takata, M.; Sakata, M.; Taninaka, A.; Shinohara, H. *Angew. Chem., Int. Ed.* **2001**, *40*, 2998–2999. (f) Shimotani, H.; Ito, T.; Iwasa, Y.; Taninaka, A.; Shinohara, H.; Nishibori, E.; Takata, M.; Sakata, M. *J. Am. Chem. Soc.* **2004**, *126*, 364–369. (g) Yamada, M.; Nakahodo, T.; Wakahara, T.; Tsuchiya, T.; Maeda, Y.; Akasaka, T.; Kako, M.; Yoza, K.; Horn, E.; Mizorogi, N.; Kobayashi, K.; Nagase, S. *J. Am. Chem. Soc.* **2005**, *127*, 14570–14571.

 10.1021/ja100665q

In this context, the first D−A conjugates based on EMFs using trimetallic nitride template EMFs (TNT-EMFs), namely $Sc_3N@I_h$-C_{80} and $Y_3N@I_h$-C_{80}, have recently been reported.[7] Importantly, in the ferrocenylpyrrolidine adduct of $Sc_3N@C_{80}$, a significant stabilization of the radical ion-pair state, formed upon irradiation, is seen when compared to an analogous C_{60}−ferrocene conjugate.[7b] This result reveals the potential of EMFs as constituents for a variety of optoelectronic devices at the nanometer scale.[7e]

On the other hand, *p*-quinonoid π-extended tetrathiafulvalenes (exTTFs) are a singular class of electron donor molecules which, unlike most known electron donors, undergo aromatization upon oxidation to afford thermodynamically stable dicationic species at relatively low oxidation potentials.[8] Moreover, the formation of aromatic species upon oxidation is accompanied by a dramatic geometrical change, from a butterfly-shaped neutral state to a planar dicationic structure, which further stabilizes the charged species. The covalent linkage of the electron-donor exTTF with electron acceptors, such as C_{60}, has allowed the preparation of a variety of photo- and electroactive dyads able to act as artificial photosynthetic systems and active molecular materials for organic photovoltaics.[9] Recently we succeeded in the realization of donor−acceptor supramolecules based on the recognition of the convex exterior of C_{60} by the concave surface of π-extended tetrathiafulvalene derivatives.[10] Numerous incentives, especially in the context of constructing more efficient optoelectronic devices, are offered by these fullerene/exTTF materials.

The first attempt to introduce exTTF donors into EMFs has recently been reported using $Y_3N@C_{80}$.[7c] The stability of the exTTF-containing $Y_3N@C_{80}$ malonate fulleroid, however, was low, and the $Y_3N@C_{80}$−exTTF dyad was oxidized spontaneously and transformed into a stable adduct containing anthraquinone, which results from the loss of the 1,3-dithiole moieties. Introducing the exTTF moiety to EMFs in a stable form would enhance the physical and photoactive functionality of the D−A conjugates by combination of their electronic properties with the singular butterfly-shape form of exTTF, particularly interesting to explore concave-convex π−π interactions. In this context, our initial interests were focused on developing a chemical modification method to obtain stable EMF derivatives endowed with exTTFs.

It is worth mentioning that $La_2@C_{80}$ and TNT−EMFs show a remarkable difference in their redox potentials as well as in the localization of their molecular orbitals.[11] Although $Sc_3N@C_{80}$ and $La_2@C_{80}$ have similar HOMO levels, $La_2@C_{80}$ has a much lower LUMO than $Sc_3N@C_{80}$. Furthermore, whereas the LUMO of $La_2@C_{80}$ is localized on the encapsulated metal atoms, those of $M_3N@C_{80}$ (M = Sc, Y, and Lu) are delocalized all over the molecule, including the fullerene cage. The localization of the electron-accepting orbital on the encapsulated metals in $M_2@C_{80}$ may impact the photoinduced intra- and/or intermolecular electron transfer dynamics.

Here, we present the first chemical derivatization of $La_2@C_{80}$ with exTTF-containing azomethine ylides to afford stable EMF-exTTF conjugates as well as the electrochemical and photophysical properties exhibited by these amphoteric redox systems. Interestingly, light irradiation promotes an efficient intramolecular electron transfer process affording the corresponding charge separated state ($La_2@C_{80}^{\bullet-}$-$exTTF^{\bullet+}$) with a lifetime in the range of a few nanoseconds.

Experimental Section

General Methods. All solvents were dried according to standard procedures. Reagents were used as purchased, unless otherwise specified. High-performance liquid chromatography (HPLC) was performed on an Agilent 1100 LC (Agilent Technologies) or an LC-9204 (Japan Analytical Industry Co., Ltd.). HPLC-grade

(3) (a) Kobayashi, K.; Nagase, S.; Maeda, Y.; Wakahara, T.; Akasaka, T. *Chem. Phys. Lett.* **2003**, *374*, 562–566. (b) Wakahara, T.; Yamada, M.; Takahashi, S.; Nakahodo, T.; Tsuchiya, T.; Maeda, Y.; Akasaka, T.; Kako, M.; Yoza, K.; Horn, E.; Mizorogi, N.; Nagase, S. *Chem. Commun.* **2007**, 2680–2682. (c) Pérez-Jiménez, Á. J. *J. Phys. Chem. C* **2007**, *111*, 17640–17645. (d) Yamada, M.; Someya, C.; Wakahara, T.; Tsuchiya, T.; Maeda, Y.; Akasaka, T.; Yoza, K.; Horn, E.; Liu, M. T. H.; Mizorogi, N.; Nagase, S. *J. Am. Chem. Soc.* **2008**, *130*, 1171–1176. (e) Yamada, M.; Wakahara, T.; Nakahodo, T.; Tsuchiya, T.; Maeda, Y.; Akasaka, T.; Yoza, K.; Horn, E.; Mizorogi, N.; Nagase, S. *J. Am. Chem. Soc.* **2006**, *128*, 1402–1403. (f) Yamada, M.; Okamura, M.; Sato, S.; Someya, I. C.; Mizorogi, N.; Tsuchiya, T.; Akasaka, T.; Kato, T.; Nagase, S. *Chem.—Eur. J.* **2009**, *15*, 10533–10542. (g) Yamada, M.; Akasaka, T.; Nagase, S. *Acc. Chem. Res.* **2010**, *43*, 92–102.

(4) For some books on fullerenes, see: (a) *Fullerenes: From Synthesis to Optoelectronic Properties*; Guldi, D. M., Martín, N., Eds.; Kluwer Academic Publishers: Dordrecht, 2002. (b) Hirsch, A. *The Chemistry of Fullerenes*; Wiley-VCH: Weinheim, 2005. (c) *Fullerenes. Principles and Applications*; Langa, F., Nierengarten, J. F., Eds.; Royal Society of Chemistry: Cambridge, 2007. (d) *Fullerene Polymers. Synthesis, Properties and Applications*; Martín, N., Giacalone, F., Eds.; Wiley-VCH: Weinheim, 2009.

(5) For reviews on C_{60}-donor composites, see: (a) Martín, N.; Sánchez, L.; Illescas, B. M.; Pérez, I. *Chem. Rev.* **1998**, *98*, 2527–2548. (b) Guldi, D. M. *Chem. Commun.* **2000**, 321–327. (c) Guldi, D. M. *Chem. Soc. Rev.* **2002**, *31*, 22–36. (d) Imahori, H. *J. Phys. Chem. B* **2004**, *108*, 6130–6143. (e) Segura, J. L.; Martín, N.; Guldi, D. M. *Chem. Soc. Rev.* **2005**, *34*, 31–47. (f) Martín, N. *Chem. Commun.* **2006**, 2093–2104. (g) Guldi, D. M.; Rahman, A. G. M.; Sgobba, V.; Ehli, C. *Chem. Soc. Rev.* **2006**, *35*, 471–487. (h) Kamat, P. V. *J. Phys. Chem. C* **2007**, *111*, 2834–2860.

(6) Gust, D.; Moore, T. A.; Moore, A. L. *Acc. Chem. Res.* **2009**, *42*, 1890–1898.

(7) (a) Chaur, M. N.; Melin, F.; Ortíz, A. L.; Echegoyen, L. *Angew. Chem., Int. Ed.* **2009**, *48*, 7514–7538. (b) Pinzón, J. R.; Plonska-Brzezinska, M. E.; Cardona, C. M.; Athans, A. J.; Gayathri, S. S.; Guldi, D. M.; Herranz, M. A.; Martin, N.; Torres, T.; Echegoyen, L. *Angew. Chem., Int. Ed.* **2008**, *47*, 4173–4176. (c) Pinzón, J. R.; Cardona, C. M.; Herranz, M. A.; Plonska-Brzezinska, M. E.; Palkar, A.; Athans, A. J.; Martín, N.; Rodríguez-Fortea, A.; Poblet, J. M.; Bottari, G.; Torres, T.; Gayathri, S. S.; Guldi, D. M.; Echegoyen, L. *Chem.—Eur. J.* **2009**, *15*, 864–877. (d) Pinzón, J. R.; Gasca, D. C.; Sankaranarayanan, S. G.; Bottari, G.; Torres, T.; Guldi, D. M.; Echegoyen, L. *J. Am. Chem. Soc.* **2009**, *131*, 7727–7734. (e) Ross, R. B.; Cardona, C. M.; Guldi, D. M.; Sankaranarayanan, S. G.; Reese, M. O.; Kopidakis, N.; Peet, J.; Walker, B.; Bazan, G. C.; Keuren, E. V.; Holloway, B. C.; Drees, M. *Nat. Mater.* **2009**, *8*, 208–212.

(8) For reviews on exTTFs chemistry and properties, see: (a) Bryce, M. R. *J. Mater. Chem.* **2000**, *10*, 589–598. (b) Segura, J. L.; Martín, N. *Angew. Chem., Int. Ed.* **2001**, *40*, 1372−1409. (c) Bendikov, M.; Wudl, F.; Perepichka, D. F. *Chem. Rev.* **2004**, *104*, 4891–4945. (d) Pérez, E. M.; Martín, N. *Chem. Soc. Rev.* **2008**, *37*, 1512–1519. (e) Pérez, E. M.; Illescas, B. M.; Herranz, M. A.; Martín, N. *New. J. Chem.* **2009**, *33*, 228–234.

(9) (a) Martín, N.; Sánchez, L.; Herranz, M. A.; Illescas, B.; Guldi, D. M. *Acc. Chem. Res.* **2007**, *40*, 1015–1024. (b) Brea, R. J.; Castedo, L.; Granja, J. R.; Herranz, M. A.; Sánchez, L.; Martín, N.; Seitz, W.; Guldi, D. M. *Proc. Natl. Acad. Sci. U.S.A.* **2007**, *104*, 5291–5294. (c) Agustín, M.-O.; Fernández, G.; Wielopolski, M.; Atienza, C.; Sánchez, L.; Gouloumis, A.; Clark, T.; Martín, N.; Guldi, D. M. *J. Am. Chem. Soc.* **2009**, *131*, 12218–12229.

(10) (a) Fernández, G.; Pérez, E. M.; Sánchez, L.; Martín, N. *Angew. Chem., Int. Ed.* **2008**, *47*, 1094−1097. (b) Fernández, G.; Pérez, E. M.; Sánchez, L.; Martín, N. *J. Am. Chem. Soc.* **2008**, *130*, 2410–2411. (c) Fernández, G.; Sánchez, L.; Pérez, E. M.; Martín, N. *J. Am. Chem. Soc.* **2008**, *130*, 10674–10683. (d) Gayathri, S. S.; Wielopolski, M.; Pérez, E. M.; Fernández, G.; Sánchez, L.; Viruela, R.; Ortí, E.; Guldi, D. M.; Martín, N. *Angew. Chem., Int. Ed.* **2009**, *48*, 815–819.

(11) (a) Iiduka, Y.; Ikenaga, O.; Sakuraba, A.; Wakahara, T.; Tsuchiya, T.; Maeda, Y.; Nakahodo, T.; Akasaka, T.; Kako, M.; Mizorogi, N.; Nagase, S. *J. Am. Chem. Soc.* **2005**, *127*, 9956–9957. (b) Cai, T.; Xu, L.; Anderson, M. R.; Ge, Z.; Zuo, T.; Wang., X.; Olmstead, M. M.; Balch, A. L.; Gilbson, H. W.; Dorn, H. C. *J. Am. Chem. Soc.* **2006**, *128*, 8581–8589.

solvents were used as the eluents. Injection volumes of samples were 25 μL for analysis and 1500 μL for preparation. The ^{1}H and ^{13}C NMR measurements were carried out on a Bruker AVANCE 300 spectrometer, a Bruker AVANCE 500 spectrometer with a CryoProbe system, or a Bruker AVANCE 700 spectrometer with a CryoProbe system, where TMS was used as an internal reference ($\delta = 0.00$ ppm). Absorption spectra were recorded with a Varian Cary 50 spectrophotometer or a SHIMADZU UV-3150 spectrophotometer. Matrix-assisted laser desorption ionization (coupled to a time-of-flight analyzer) experiments (MALDI-TOF) were recorded on a Bruker BIFLEX III. Cyclic voltammograms (CVs) and differential pulse voltammograms (DPVs) were recorded on a BAS CV50W electrochemical analyzer. Platinum wires were used as the working and counter electrodes. The reference electrode was a saturated calomel reference electrode (SCE) filled with 0.1 M (n-Bu)$_4$NPF$_6$ (TBAPF$_6$) in o-DCB. All potentials are referenced to the ferrocene/ferrocenium couple (Fc/Fc$^+$) as the internal standard. CVs were recorded using a scan rate of 50 mV/s, and DPVs were obtained using a pulse amplitude of 50 mV, a pulse width of 50 ms, a pulse period of 200 ms, and a scan rate of 20 mV/s. The solution was deaerated for 20 min with argon prior to the electrochemical measurements. Femtosecond transient absorption studies were performed with 387 nm laser pulses (1 kHz, 150 fs pulse width, 200 nJ) from an amplified Ti:Sapphire laser system (Model CPA 2101, Clark-MXR Inc.). Pulse radiolysis experiments were performed using 50 ns pulses of 15 MeV electrons from a LINAC linear electron accelerator. Dosimetry was based on the oxidation of SCN$^-$ to (SCN)$_2^{\bullet -}$, which in N_2O-saturated aqueous solution takes place with $G \approx 6$ (G denotes the number of species per 100 eV, or the approximate μM concentration per 10 J absorbed energy). The radical concentration generated per pulse was varied over the range $1-3 \times 10^{-6}$ M.

2-Formyl-9,10-bis(1,3-dithiol-2-ylidene)-9,10-dihydroanthracene (exTTF-CHO)[12] and *N*-(2-ethylhexyl)glycine ($C_5H_{10}C_2H_5CH_2NHCH_2COOH$)[13] were synthesized according to the reported procedures.

General Procedure for the Synthesis of Pyrrolidine Adducts 1−3. A toluene solution containing La$_2$@I_h-C$_{80}$ was refluxed with 5.0 equiv of the corresponding glycine and aldehyde under argon atmosphere. After a variable period of time, the reaction mixture was injected into a preparative Buckyprep column (20 mm $\times$250 mm i.d.; Cosmosil, Nacalai Tesque, Inc.) to separate **1−3** from byproducts and unreacted starting materials.

La$_2$@C$_{80}$CH$_2$NEtCHPh (1). La$_2$@I_h-C$_{80}$ (4.00 mg, 1.08×10^{-4} M) was dissolved in 40 mL of toluene and refluxed for 1 h after the addition of 1.67 mg of *N*-ethylglycine and 1.71 mg of benzaldehyde: 77% yield (based on consumed starting La$_2$@I_h-C$_{80}$); ^{1}H NMR (300 MHz, CS$_2$/C$_2$D$_2$Cl$_4$, 3/1, 253 K) δ 7.89 (Ph, d, 2H, $J = 8.1$ Hz), 7.61−7.31 (Ph, m, 3H), 4.42 (d, 1H, $J = 9.5$ Hz), 3.94 (CH, s, 1H), 3.08 (brs, 1H), 3.02 (d, 1H, $J = 9.5$ Hz), 2.22 (brs, 1H), 0.83 (CH$_3$, brs, 3H); ^{13}C NMR (125 MHz, CS$_2$/C$_2$D$_2$Cl$_4$, 3/1, 283 K) δ 154.2, 152.7, 150.4, 148.6, 146.7, 146.0, 145.2, 144.5 (2C), 144.0, 143.8, 143.4 (2C), 142.8, 142.6 (4C), 142.5, 141.4, 140.9 (2C), 140.8 (2C), 140.1 (2C), 139.8 (2C), 139.7 (3C), 139.3, 139.2 (4C), 138.9 (3C), 138.5 (2C), 138.4 (2C), 138.1, 137.8 (2C), 137.3 (2C), 137.2 3C), 136.9, 136.8 (3C), 136.4 (3C), 136.3 (2C), 136.0 (2C), 135.9, 135.7, 135.7, 135.4, 135.3 (3C), 135.2 (2C), 135.1, 134.8, 132.5, 130.2, 130.1, 129.4 (CH), 128.8, 128.8 (CH), 128.7 (CH), 128.5 (CH), 128.4 (CH), 128.1, 125.2, 87.3 (pyrrolidine CH), 71.1 (pyrrolidine CH$_2$), 64.2 (sp^3 on cage), 57.8 (sp^3 on cage), 46.7 (NCH$_2$), 13.4 (CH$_3$); MALDI-TOF MS calcd for $C_{90}H_{13}La_2N$ ([M]$^-$) 1384.92, found 1385.68.

La$_2$@C$_{80}$CH$_2$NEtCHexTTF (exTTF = C$_{20}$H$_{11}$S$_4$) (2). La$_2$@I_h-C$_{80}$ (1.00 mg, 1.08×10^{-4} M) was dissolved in 10 mL of toluene and refluxed for 1 h after the addition of 0.42 mg of *N*-ethylglycine and 1.65 mg of exTTF-CHO:[12] 68% yield (based on consumed starting fullerene); ^{1}H NMR (500 MHz, CS$_2$/C$_2$D$_2$Cl$_4$, 3/1, 258 K) δ 8.20 (s, 1H), 7.75−7.61 (m, 4H), 7.29−7.23 (m, 2H), 6.35 (d, 1H, $J = 6.5$ Hz), 6.33 (d, 1H, $J = 6.5$ Hz), 6.29 (d, 1H, $J = 6.5$ Hz), 6.19 (d, 1H, $J = 6.5$ Hz), 4.46 (d, 1H, $J = 9.3$ Hz), 4.07 (s, 1H), 3.11 (d, 1H, $J = 9.3$ Hz), 3.03 (brs, 1H) 2.24 (brs, 1H) 0.87 (CH$_3$, brs, 3H); UV−vis-NIR (toluene) λ_{max} 363, 415, 431 nm; MALDI-TOF MS calcd for $C_{104}H_{19}La_2NS_4$ ([M]$^-$) 1686.85, found 1686.83.

La$_2$@C$_{80}$CH$_2$NC$_8$H$_{17}$CHexTTF (3). La$_2$@I_h-C$_{80}$ (4.00 mg, 1.08×10^{-4} M) was dissolved in 40 mL of toluene and refluxed for 2 h after the addition of 3.03 mg of *N*-(2-ethylhexyl)glycine[13] and 6.60 mg of exTTF-CHO:[12] 70% yield (based on consumed starting fullerene); ^{1}H NMR (500 MHz, CS$_2$/C$_2$D$_2$Cl$_4$, 3/1, 273 K) δ 8.26 (s, 1H), 7.70−7.61 (m, 4H), 7.29−7.26 (2H), 6.35 (d, 1H, $J = 6.8$ Hz), 6.33 (d, 1H, $J = 6.8$ Hz), 6.29 (d, 1H, $J = 6.8$ Hz), 6.19 (d, 1H, $J = 6.8$ Hz), 4.45 (d, 1H, $J = 10.0$ Hz), 4.04 (s, 1H), 3.02 (d, 1H, $J = 10.0$ Hz), the proton signals due to the alkyl side chain (C$_8$H$_{17}$) could not be identified; ^{13}C NMR (175 MHz, CS$_2$/C$_2$D$_2$Cl$_4$, 3/1, 293 K) δ 154.1, 153.3 149.9, 148.5, 146.4 (2C), 146.1, 145.4, 145.2 (2C), 145.0, 144.9, 144.8, 144.7, 143.8, 143.6, 143.4 (2C), 143.3, 142.8 (2C), 142.7 (3C), 141.9 (2C), 141,7,141.4 (2C), 141.3 (2C), 141.2, 140.7, 140.7, 140.2, 139.9, 139.8, 139.6 (2C), 139.4, 139.2 (2C),139,1 (2C), 138.6, 138.3, 137.9 (2C), 137.7,137.6, 137.5, 137.4, 137.2 (2C), 137.1, 136.6 (2C), 136.5 (2C), 136.3, 136.2, 136.0 (2C), 135.8,135.6, 135.5, 135.4, 135.3 (2C), 135.2, 135.1 (2C), 134.9, 134.8 (2C), 134.3, 133.4 (2C), 132.6 (2C), 130.5, 129.7 (2C), 128.9, 128.8 (CH), 128.1 (CH), 127.8 (CH), 126.0(CH), 125.2 (CH), 125.0 (CH), 124.8 (CH), 120.3, 117.4 (SCH), 117.3 (2SCH), 117.2 (SCH), 88.5 (pyrrolidine CH), 72.2 (pyrrolidine CH$_2$), 64.2 (sp^3 on cage), 57.2 (sp^3 on cage), the carbon signals due to the alkyl side-chain (C$_8$H$_{17}$) could not be identified; UV−vis−NIR (toluene) λ_{max} 363, 416, 430 nm; MALDI-TOF MS calcd for $C_{110}H_{31}La_2NS_4$ ([M]$^-$) 1771.95, found 1772.90.

Results and Discussion

La$_2$@C$_{80}$ was successfully functionalized by 1,3-dipolar cycloaddition reaction of azomethine ylides—generated *in situ* from 5 equiv of precursor amino acid and aldehyde components—in refluxing toluene for a few hours (Scheme 1).[14] The HPLC profiles of the resulting crudes showed sharp peaks corresponding to the novel cycloadducts of La$_2$@C$_{80}$ (**1−3**) (see Figure 1 and Supporting Information). Resemblance in HPLC profiles among **1−3** suggests their similar reactivities regardless the choice of the starting aminoacids and aldehydes. In order to increase the solubility of the dyads, for further photophysical investigation in different solvents, we synthesized compound **3** bearing a solubilizing alkyl chain on the pyrrolidine nitrogen atom. **1−3** were isolated from the respective reaction mixture by one-step HPLC separation. Storing **1−3** in toluene solutions under ambient and light-shielding conditions for a week did not show any change in the retention time of HPLC profiles, thus indicating that oxidation of the compounds do not occur easily (not shown). The matrix-assisted laser desorption ionization time-of-flight (MALDI-TOF) mass spectra of **1−3**, under negative ionization conditions, show strong molecular ion peaks with fragment peaks during the laser desorption process (Figure S3, Supporting Information).

UV−vis−NIR spectra of **1−3** show characteristic absorptions (Figure 2). Since two types of C=C double bonds are available on the La$_2$@I_h-C$_{80}$ cage, two regioisomers can be formed by cycloaddition reaction, namely [6,6] and [5,6] cycloadducts. The

(12) Martín, N.; Pérez, I.; Sánchez, L.; Seoane, C. *J. Org. Chem.* **1997**, *62*, 5690–5695.
(13) Hanabusa, K.; Suzuki, M.; Saito, K.; Hattori, T. Patent no. JP2008222759.
(14) (a) Maggini, M.; Scorrano, G.; Prato, M. *J. Am. Chem. Soc.* **1993**, *115*, 9798–9799. (b) Tagmatarchis, N.; Prato, M. *Synlett* **2003**, 768–779. (c) Tasis, D.; Tagmatarchis, N.; Bianco, A.; Prato, M. *Chem. Rev.* **2006**, *106*, 1105–1136.

Scheme 1

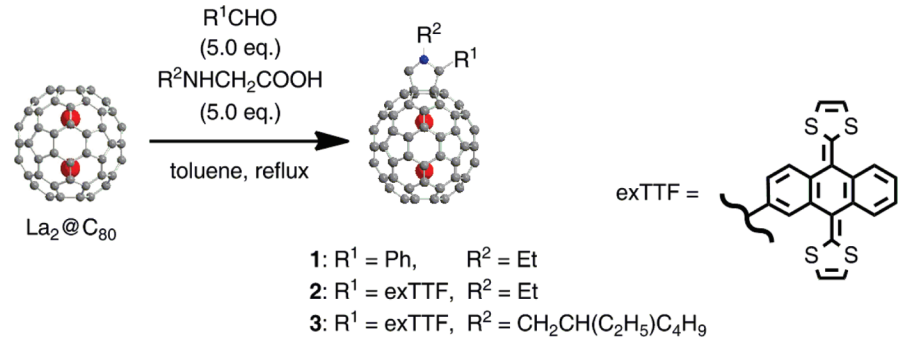

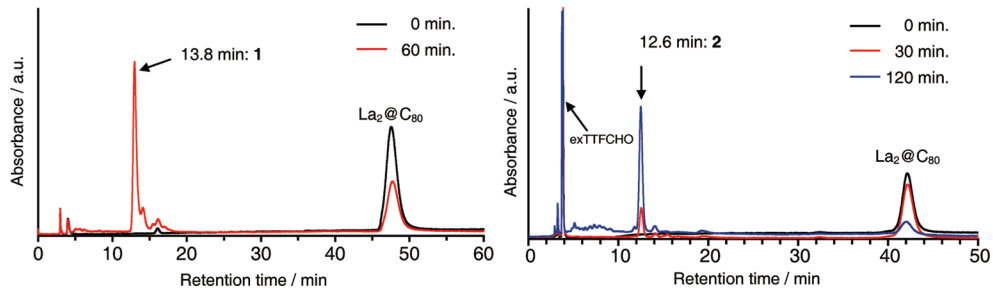

Figure 1. HPLC profiles of the reaction crudes of **1** (left) and **2** (right). Conditions: Buckyprep column (φ 4.6 mm × 250 mm); eluent, toluene; flow rate, 1.0 mL/min; wavelength, 330 nm; temperature, room temperature for **1** and 40 °C for **2**.

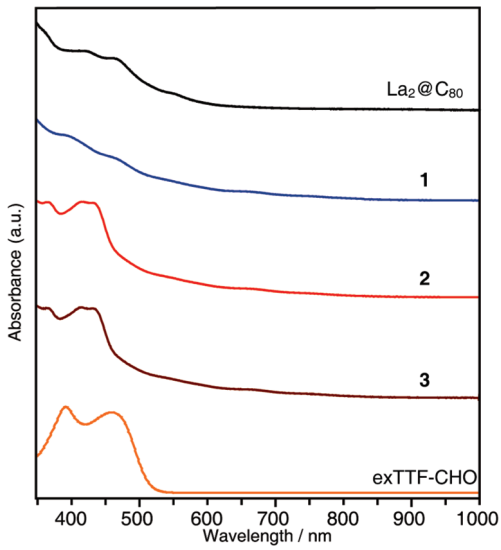

Figure 2. UV−vis−NIR absorption spectra of **1**−**3**, $La_2@C_{80}$, and exTTF-CHO in toluene.

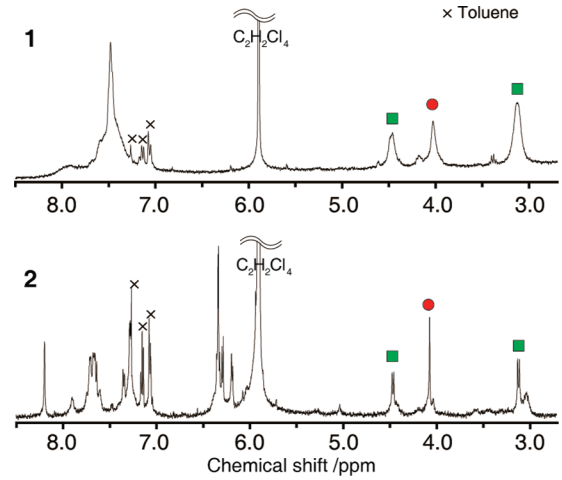

Figure 3. ^{1}H NMR spectra of **1** (top) at 300 MHz and **2** (bottom) at 500 MHz, in 1:3 (v/v) $C_2D_2Cl_4/CS_2$ at 293 K. The signals marked by green squares and red circles are due to the pyrrolidine geminal and methine protons, respectively.

spectrum of **1**, however, reveals striking similarities in the UV−vis−NIR region to that of the previously reported analog [5,6] cycloadduct of $La_2@C_{80}$.[3f] The electronic spectra of fullerene derivatives usually provide sufficiently distinctive fingerprints of the π-electron system topology. Therefore, it is reasonable to conclude that the found similarities between the spectra of **1** and the [5,6] adduct implies the isostructural nature of the respective compounds, that is, the same addition pattern of the substituents. This conclusion is also supported by the experimental results in NMR and CV/DPV measurements mentioned below.

For **2** and **3**, strong absorption bands around 420 nm due to the presence of the exTTF moiety were found as additional peaks to the spectral pattern of [5,6] metallofulleropyrrolidines as shown in **1**.

The ^{1}H NMR spectrum of **1** clearly shows only one set of signals for the pyrrolidine proton, thus indicating the presence of a single regioisomer resulting from the cycloaddition reaction (Figure 3). The signals for the pyrrolidine geminal protons appeared as doublets at δ 4.42 and δ 3.02 (J = 9.5 Hz), while the remaining pyrrolidine methine proton is observed as a singlet signal at δ 3.94. The chemical shifts of the geminal protons are quite similar to those previously reported for pyrrolidine [5,6] cycloadducts of $La_2@C_{80}$ and distinct from those for the [6,6] cycloadduct.[3f] On the other hand, the fact that the signal from one of the methylene protons (δ 4.42) appears downfielded compared to the methine proton may be ascribed to the strong deshielding ring current effect on the methylene proton.

Regarding ^{1}H NMR spectra of **2** and **3**, the signals corresponding to the pyrrolidine protons were observed at similar

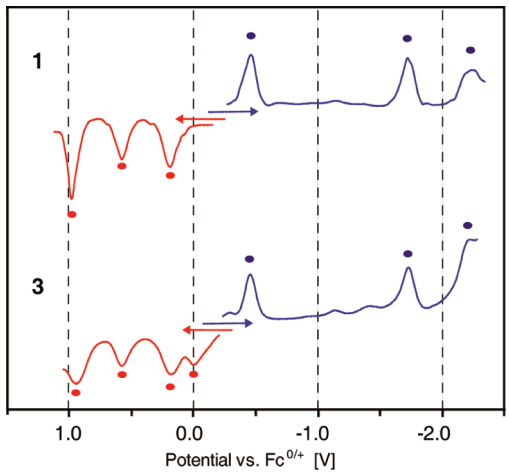

Figure 4. DPVs of **1** (top) and **3** (bottom) measured in *o*-DCB at room temperature.

Table 1. Redox Potentials[a,b]

compd	$E_{ox}^{(4)}$	$E_{ox}^{(3)}$	$E_{ox}^{(2)}$	$E_{ox}^{(1)}$	$E_{red}^{(1)}$	$E_{red}^{(2)}$	$E_{red}^{(3)}$
1		1.00[c]	0.59	0.20	−0.44	−1.70	−2.22[c]
3	0.95[c]	0.58	0.19	0.00	−0.45	−1.73	−2.23[c]
exTTF-CHO				0.06			
5,6-$La_2@C_{80}(CH_2)_2NTrt$[d]		1.01[c]	0.63	0.23	−0.45	−1.71	−2.30[c]
6,6-$La_2@C_{80}(CH_2)_2NTrt$[d]			0.95[c]	0.55	−0.51	−1.65	−2.19[c]
$La_2@C_{80}$[e]			0.95[c]	0.56	−0.31	−1.71	−2.13[c]

[a] Values are given in volts relative to a $Fc^{0/+}$ redox couple and were obtained from DPVs. [b] Conditions: working electrode and counter electrode, platinum wires; reference electrode, SCE; supporting electrolyte, 0.1 M $TBAPF_6$ in *o*-DCB. CV: scan rate, 50 mV s^{-1}. DPV: pulse amplitude, 50 mV; scan rate, 20 mV s^{-1}. [c] Irreversible. [d] Data from ref 3f. [e] Data from ref 2b.

magnetic field regions to those of **1** (Figure 3). In addition, the resonances for the aromatic protons of the anthracenyl group in the exTTF moiety appear between δ 8.3 and δ 7.2, and the signals of the two 1,3-dithiole rings appear in the region of δ 6.4−6.2, for both **2** and **3**. The H−H COSY spectrum of **2** (Figure S4, Supporting Information) ensures the coupling between the protons, thus confirming the proposed structure.

Temperature-dependent ^{1}H NMR spectra were also recorded for **1** and **2**. Proton signals were sharpened and complicated with decreasing temperature below 260 K, which indicates a decelerating of the flip-flap motions of the pyrrolidine rings (Figure S5, Supporting Information).

^{13}C NMR spectra of **1** and **3**, show a total of 80 lines for the C_{80} cage in both compounds, thus indicating the C_1 symmetry of the endohedral fullerene cage (Figure S6, Supporting Information). The signals due to the sp^3 carbon atoms of the pyrrolidine ring appear at δ 64.2 and δ 57.8 for **1**, and 64.2 and 57.2 for **3**, confirming their [5,6]-closed structures. HSQC measurement on **3** reveals the couplings between the carbon atoms and the protons of the exTTF moiety between δ 128−117 (Figure S7, Supporting Information).

Differential pulse voltammetry (DPV) and cyclic voltammetry (CV) experiments were carried out on compounds **1** and **3** in *o*-DCB solutions at room temperature (Figure 4 and Figure S8, Supporting Information). The redox potentials of **1**, **3**, exTTF-CHO,[12] and [5,6]- and [6,6]metallofulleropyrrolidines of $La_2@C_{80}$−$(CH_2)_2NTrt$[3f] and $La_2@C_{80}$[2b] are shown in Table 1. Two one-electron reversible reduction waves at −0.44 and −1.70 V vs Fc/Fc^+ are observed for **1**. In the oxidation side, two reversible processes are found at +0.20 and +0.59 V, indicating the formation of a [5,6]pyrrolidine derivative of $La_2@C_{80}$.[3f] For **3**, reduction potentials are almost identical to those of **1**, and cathodically shifted by ca. 130−140 mV compared to $La_2@C_{80}$. This experimental finding has been accounted for by the raising of the LUMO due to the saturation of a double bond of the fullerene cage.[7a] On the other hand, the first oxidation process at +0.00 V is unambiguously assigned to the exTTF moiety, followed by the three oxidation processes at +0.19, +0.58, and +0.95 V corresponding to the fullerene cage. The redox potentials, as found for **3**, reveal, in agreement with the data stemming from the electronic spectra, only weak electronic interactions between the redox chromophores in their ground state.

On the basis of the observations in ^{1}H, ^{13}C NMR, UV−vis−NIR spectra, and CV/DPV measurements, **1**−**3** could be assigned to single regioisomers with [5,6]-closed structure.[15] In contrast, we have recently reported the functionalization of $M_2@C_{80}$ (M = La or Ce) based on *N*-tritylazomethine ylide by an exclusion of carbon dioxide from 3-triphenylmethyl-5-oxazolidinone, affording both [5,6] and [6,6] regioisomers.[3f] In comparison to that case, functionalization of $La_2@C_{80}$ with *N*-alkylazomethine ylides shows a higher regioselectivity in the addition reaction.

Similar results have recently been reported by Dorn *et al.* on the regioselective cycloaddition of azomethine ylides to TNT-EMFs. Both the [6,6] and [5,6] pyrrolidine monoadducts of $Sc_3N@C_{80}$ were isolated when an *N*-trityl azomethine ylide was employed instead of the *N*-methyl or *N*-ethyl analogues.[16] These experimental results, underpinned by computational studies by Echegoyen and Poblet, seem to indicate that a pirouette-kind mechanism gives rise to the thermodynamically favored [5,6] monoadducts, from the kinetically preferred products.[17] It was concluded that the rate of this rearrangement depends on the internal cluster and on the pyrrolidine addend. In accord with this conclusion, the use of $La_2@C_{80}$ and *N*-alkylazomethine ylides leads to [5,6] monoadducts in a highly regioselective way.

To evaluate excited-state interactions, as a complement to the above-described ground state interactions, we investigated first the emissive properties of **3** in relation to its references (i.e., $La_2@C_{80}$ and exTTF). For exTTF, a broad and featureless emission pattern ranging from 450 to 760 nm is seen in the steady-state emission experiments. Successful determination of the corresponding emission lifetime is, however, hampered by the instrumental time resolution of our experimental setup (i.e., about 100 ps). In **3**, a similar exTTF related emission pattern evolves. A comparison of the emission from exTTF with that of **3** revealed no appreciable quenching (Figure S9, Supporting Information). In stark contrast, $La_2@C_{80}$-centered emission were not detected neither in the reference nor in **3**.

In addition, the novel electron donor−acceptor hybrid (**3**) and its references (i.e., $La_2@C_{80}$ and exTTF) were subjected to pump probe experiments using 387 nm as excitation wavelength; see Figures 5−8.

Photoexcitation of exTTF generates an exTTF-centered excited state. Spectral characteristics of this very short-lived excited state are transient maxima around 530 nm as well as transient bleaching at <450 nm (Figure 5). Due to strong second-

(15) Cardona, C. M.; Elliott, B.; Echegoyen, L. *J. Am. Chem. Soc.* **2006**, *128*, 6480–6485.
(16) Cai, T.; Slebodnick, C.; Xu, L.; Harich, K.; Glass, T. E.; Chancellor, C.; Fettinger, J. C.; Olmstead, M. M.; Balch, A. L.; Gibson, H. W.; Dorn, H. C. *J. Am. Chem. Soc.* **2006**, *128*, 6486–492.
(17) Rodríguez-Fortea, A.; Campanera, J. M.; Cardona, C. M.; Echegoyen, L.; Poblet, J. M. *Angew. Chem., Int. Ed.* **2006**, *45*, 8176−8180.

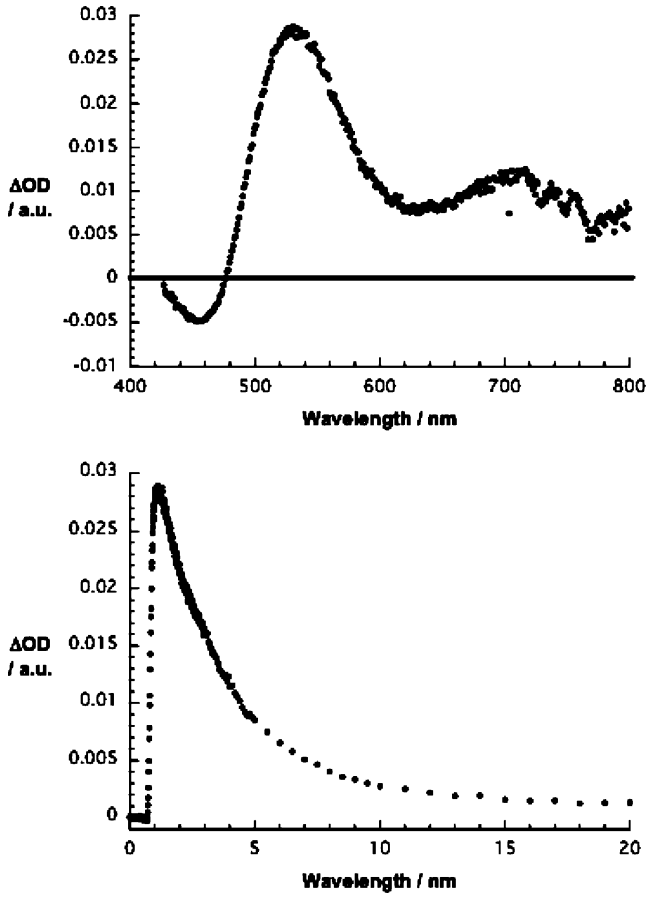

Figure 5. (Top) differential absorption spectrum (visible) obtained upon femtosecond flash photolysis (387 nm) of exTTF ($\sim 10^{-5}$ M) in argon-saturated THF with a time delay of 1 ps at room temperature. (Bottom) time–absorption profile of the spectrum shown above at 530 nm monitoring the formation and decay of the excited state.

order spin couplings,[18] exTTF centered excited states decay—even in the absence of an electron acceptor—quickly, that is, within the time window of up to approximately 20 ps with a rate constant of 2×10^{11} s^{-1} to regenerate the singlet ground state quantitatively.

When turning to $La_2@C_{80}$ the following singlet excited features emerge: maxima at 520, 580, and 1110 nm. This singlet excited state, as depicted in Figure 6, is, however, subject to a rapid intersystem crossing (3×10^{10} s^{-1}) regardless of the solvent polarity (i.e., toluene, THF, or benzonitrile) to yield the energetically lower lying triplet excited state. For the latter, we noted a several nanosecond-lived transient maximum at 500 nm.

In the electron donor−acceptor conjugate (**3**), considering the absorption features of both constituents at 387 nm, we must assume that $La_2@C_{80}$ and exTTF both get excited. Evidence for this assumption was borrowed from the transient absorption spectra as they develop, for example, in THF at time delays close to the initial excitation, namely up to 5 ps. To be precise, in the visible region (i.e., 400−800 nm) we noticed short-lived features around 530 nm that are associated with the excited-state features of exTTF; compare Figures 5 and 7. When turning to the near-infrared region (i.e., 800−1400 nm), a broad transient

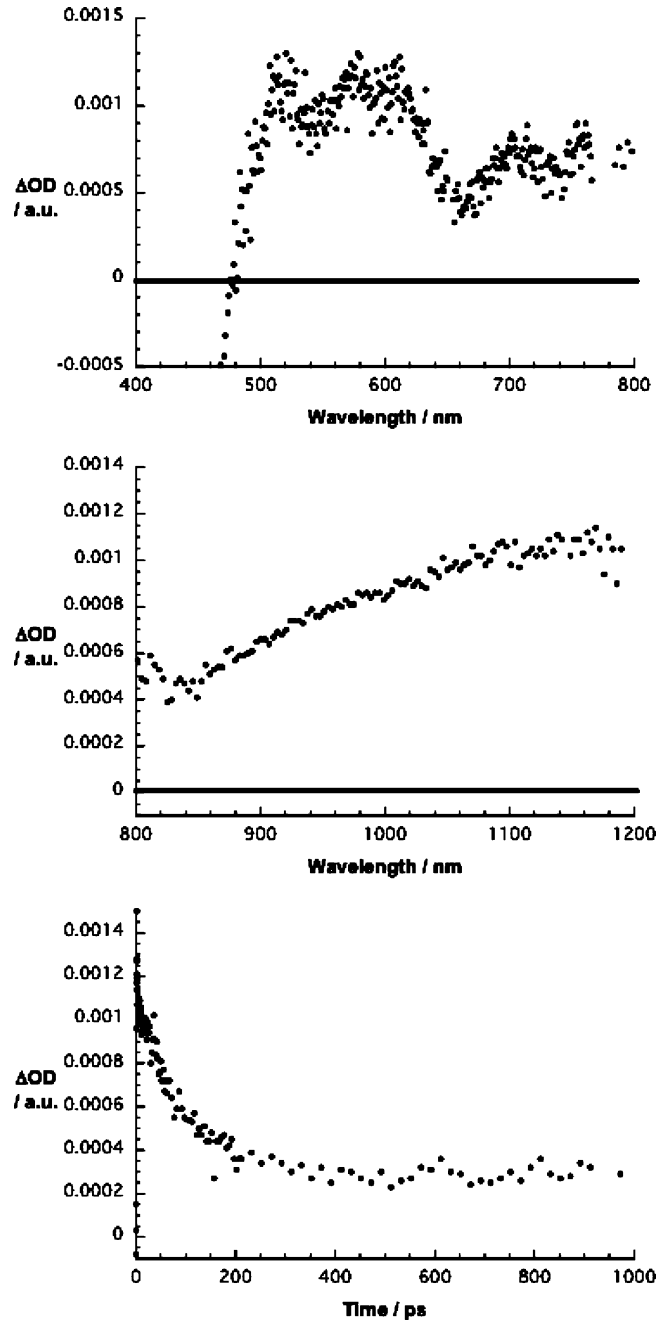

Figure 6. (Top) differential absorption spectrum (visible) obtained upon femtosecond flash photolysis (387 nm) of $La_2@C_{80}$ ($\sim 10^{-5}$ M) in argon-saturated THF with a time delay of 10 ps at room temperature. (Middle) differential absorption spectrum (near-infrared) obtained upon femtosecond flash photolysis (387 nm) of $La_2@C_{80}$ ($\sim 10^{-5}$ M) in argon-saturated THF with a time delay of 10 ps at room temperature. (Bottom) time−absorption profile of the spectrum shown above at 1150 nm monitoring the formation and decay of the excited state.

is detected that bears great resemblance with that seen for $La_2@C_{80}$; compare Figures 6 and 7. Common to the visible and near-infrared characteristics in **3**, namely the maxima at 530 and 1300 nm, is a monoexponential decay as documented in Figure 7. Here, a global analysis leads to a rate constant of 6.0×10^{10} s^{-1}. A closer look at the absorption characteristics sheds light onto the nature of the photoproduct that evolves as a consequence of the fast excited state decay. Again, in the visible range, we note an absorption that corresponds unambiguously to the marker of the one-electron oxidized exTTF. The radical

(18) (a) Maciejewski, R. P.; Steer, R. P. *Chem. Rev.* **1993**, *93*, 67–98. (b) Nishikawa, H.; Kojima, S.; Kodama, T.; Ikemoto, I.; Suzuki, S.; Kikuchi, K.; Fujitsuka, M.; Luo, H.; Araki, Y.; Ito, O. *J. Phys. Chem. A* **2004**, *108*, 1881–1890.

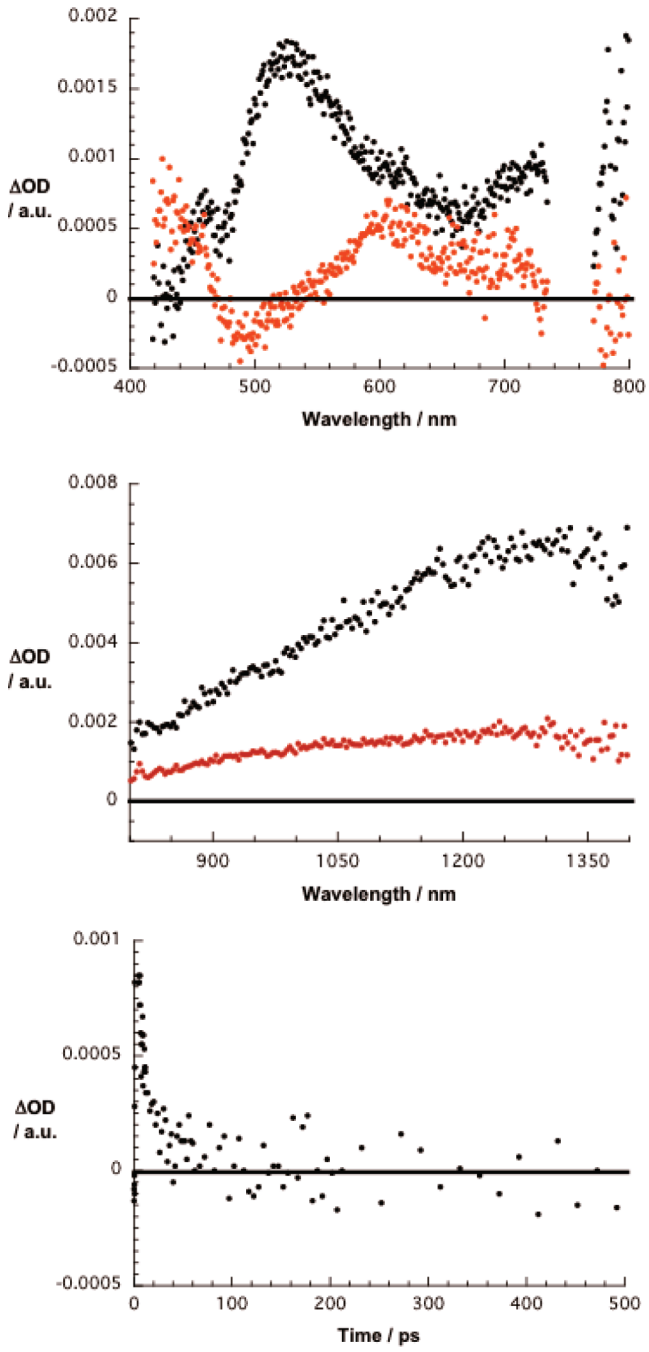

Figure 7. (Top) differential absorption spectra (visible) obtained upon femtosecond flash photolysis (387 nm) of **3** ($\sim 10^{-5}$ M) in argon-saturated THF with time delays of 5 ps (black spectrum) and 10 ps (red spectrum) at room temperature. (Middle) differential absorption spectra (near-infrared) obtained upon femtosecond flash photolysis (387 nm) of **3** ($\sim 10^{-5}$ M) in argon-saturated toluene with time delays of 5 ps (black spectrum) and 10 ps (red spectrum) at room temperature. (Bottom) time−absorption profiles of the spectra shown above at 520 nm monitoring the charge separation.

cation absorption maximizes in the current case at 610 nm, a value that is in excellent agreement with previous pulse radiolytic investigations.[9a,10d] The reduction of fullerenes is typically associated with characteristic changes in the near-infrared region around 1200 nm. Implicit are the absorption pattern of the one-electron reduced form that depends on the nature of the fullerene and the specific addition pattern of the fullerene derivatives. Notable is that the ground-state absorption of $La_2@C_{80}$ lacks like what has been seen, for example, for

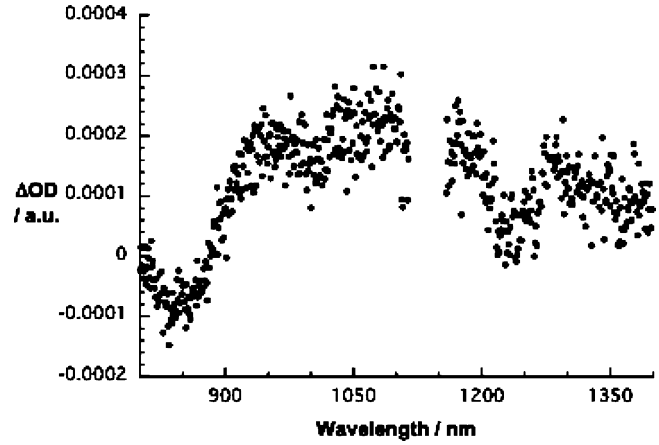

Figure 8. Differential absorption spectrum (visible and near-infrared) obtained upon electrochemical reduction of a $La_2@C_{80}$ reference at an applied bias of −0.5 V in argon-saturated *o*-dichlorobenzene at room temperature (i.e., platinum gauze working electrode; platinum wire counter electrode; silver wire as pseudo reference electrode; tetrabutylammonium perchlorate supporting electrolyte).

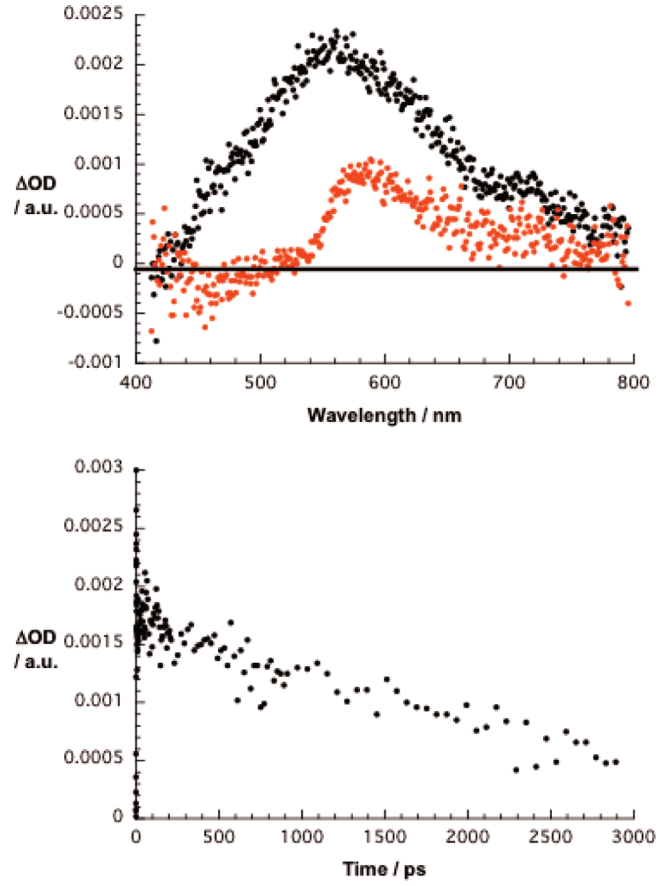

Figure 9. (Top) differential absorption spectra (visible and near-infrared) obtained upon femtosecond flash photolysis (387 nm) of **3** ($\sim 10^{-5}$ M) in argon-saturated toluene with time delays of 5 ps (black spectrum) and 10 ps (red spectrum) at room temperature. (Bottom) time−absorption profiles of the spectra shown above at 570 nm monitoring the charge separation and charge recombination.

C_{60}, C_{70}, etc.,[19] transitions in the near-infrared region. As a matter of fact, we see at times absorptions that relate to the formation of the radical cation of exTTF in the visible range (i.e., 400−800 nm) and a transient maximum in the near-infrared window (i.e., 800 and 1500 nm). The maximum is centered

around 1200 nm. We ascribe this change in oscillator strength to the reduction of $La_2@C_{80}$. Of particular importance is the close resemblance of the near-infrared part with the radiolytically and spectroelectrochemically generated spectrum of the one-electron reduced form of $La_2@C_{80}$ (Figure 8). Taking the aforementioned together, we reach the important conclusion that upon photoexciting **3** in THF a rapid intramolecular decay leads to the formation of a radical ion pair state, namely $La_2@C_{80}^{\bullet-}-exTTF^{\bullet+}$. Figure 9 illustrates that a quantitative similar picture evolves in the less polar toluene with kinetics that are virtually superimposable to those in THF. Once again, charge transfer (5.0×10^{10} s^{-1}) is the operative mode to deactivate photoexcited **3** and to form $La_2@C_{80}^{\bullet-}-exTTF^{\bullet+}$. From the corresponding time−absorption profile, a lifetime of 3260 ps (3.0×10^8 s^{-1}) was derived for the $La_2@C_{80}^{\bullet-}-exTTF^{\bullet+}$ radical ion-pair state.

Conclusion

In summary, a novel electron donor−acceptor conjugate based on an endohedral rare earth metallofullerene and exTTF was successfully synthesized, isolated, and characterized. Importantly, spectroscopic analyses and electrochemical investigation corroborate that the main product of the 1,3-dipolar cycloaddition reaction, based on the *N*-alkylazomethine ylides, is the [5,6] regioisomer. Absorption measurements in the visible and near-infrared region complemented by CV−DPV measurements are the basis for the hypothesis that the ground state is characterized by weak interactions between the photo- and redox-active constituents. Unlike the ground state, the excited state is subject to sizable interactions between the electron acceptor and the electron donor. In fact, a rapidly evolving charge transfer transforms the initial excited state into a nanosecond-lived radical ion-pair state.

Acknowledgment. Financial support from the Deutsche Forschungsgemeinschaft (SFB 583), the Volkswagen Foundation (I-77/855), a Grant-in-Aid for Scientific Research on Innovation Areas (No. 20108001, "pi-Space"), a Grant in-Aid for Scientific Research (A) (No. 20245006), The Next Generation Super Computing Project (Nanoscience Project), Nanotechnology Support Project, and a Grant-in Aid for Scientific Research on Priority Area (Nos. 20036008, 20038007, 20045002) from the Ministry of Education, Culture, Sports, Science, and Technology of Japan is acknowledged. Support from the MICINN of Spain (projects CTQ2008-00795 and Consolider-Ingenio 2010 CSD2007-0010, Nanociencia Molecular) and the CAM (Project S2009/PPQ-1533, MADRISOLAR-2) is greatly appreciated.

Supporting Information Available: HPLC profiles of the reaction crude of **3** and isolated **1**−**3**, MALDI TOF mass spectra of **1**−**3**, H−H COSY spectrum of **2**, ^1H and ^{13}C NMR spectra for **1** and **3**, HSQC spectrum of **3**, CVs of **1** and **3**, and emission spectra of exTTF and **3**. This material is available free of charge via the Internet at http://pubs.acs.org.

JA100665Q

(19) (a) Ajie, H.; Alvarez, M. M.; Anz, S. J.; Beck, R. D.; Diederich, F.; Fostiropoulus, K.; Huffman, D. R.; Krätschmer, W.; Rubin, Y.; Schriver, K. E.; Sensharma, D.; Whetten, R. L. *J. Phys. Chem.* **1990**, *94*, 8630–8633. (b) Suzuki, I.; Tsuboi, Y.; Miyasaka, H.; Itaya, A. *Bull. Chem. Soc. Jpn.* **2000**, *73*, 589–598. (c) Shinohara, H. *Rep. Prog. Phys.* **2000**, *63*, 843–892. (d) Fujitsuka, M.; Ito, O.; Kobayashi, K.; Nagase, S.; Yamamoto, K.; Kato, T.; Wakahara, T.; Akasaka, T. *Chem. Lett.* **2000**, *8*, 902–903.